Power Research - A Journal of CPRI, Vol 22(1), 2026 | pp. 67-76

Wide-Area Assessment of Transient Stability Using Synchrophasors for IBR Integrated Power Grids

Adnan Iqbal*, Vedanta Pradhan and O. D. Naidu

Hitachi Energy Research, 8th Floor, Brigade Opus, No. 70/401, Kodigehalli Main Road, Sanjeevini Nagar, Bengaluru - 560092, Karnataka, India; adnan.iqbal@hitachienergy.com

Keywords: Blackouts, Grid Following, Inertial Control, Renewables, Synchrophasors, Transient Stability Assessment, Wide-Area Monitoring

Article Received: 30-01-2026
Article Revised: 09-02-2026
Article Accepted: 23-02-2026

DOI: 10.33686/pwj.22.1.2026.67-76

*Author for Correspondence

Abstract

Blackouts compromise grid security and are detrimental to the economics of power system operation. Clean and cheaper electricity from renewable sources has gained massive adoption globally, however, the rapid adoption of renewables comes at the expense of reduced system strength and inertia, and introduces complex dynamics due to possible interactions between the grid and inverter-based generation. Therefore, assessing system stability during severe grid contingencies has become increasingly important. The paper discusses the assessment of transient stability using a method called the "Phasor Area Criterion" for power systems integrated with inverter-based resource, and examines practical grid events such as the 8th January 2021 European system separation event. The results demonstrate the effectiveness of PAC in assessing transient stability for the simulated and real-world grid events.

This is an open access article under the terms of the CC BY: Allows others to copy, distribute, and build upon the work for any purpose, provided they credit the original creator

© 2026 The Author(s). *Central Power Research Institute* published by Informatics Publishing Limited

1. INTRODUCTION

Due to the significant economic, social, and environmental benefits of renewable energy, nations worldwide are committing to achieve aggressive renewable penetration targets[1]. This transition has led to an increased integration of Inverter-Based Resources (IBRs), which adds uncertainty to the grid's dynamics and abates the natural inertial response of the system. The reduction in system inertia directly reduces the overall transient stability margin, rendering the power system increasingly vulnerable to transient instability following sudden disturbances.

The 2012 Indian blackout affected 600 million people[2], the North East blackout of 2003 in the United States impacted 50 million[3], and the 2006 European blackouts affected 10 million[4]. These large-scale outages result in substantial financial implications due to productivity loss, equipment damage, and high emergency restoration costs. Consequently, there is a pressing need for real-time situational awareness tools to monitor transient stability status and provide timely alerts to System Operators (SOs) regarding the impact of an event, thereby aiding in preventing its spread[5,6]. Recent grid events such as blackouts and system separations underscore the severity of such vulnerable scenarios. The European Network of Transmission System Operators for Electricity (ENTSO-E) reported a significant angular separation of the European continent into two areas on 8th January 2021 and 24th July 2021, respectively[7,8]. More recently, the Spain blackout of 2025 further demonstrated the susceptibility of modern grids to severe grid contingencies. Such contingencies are not isolated, but a series of wide-area correlated cascading phenomenons that drives the system towards instability[9].

A primary challenge in Transient Stability Assessment (TSA) is that rotor angles are not directly observable and are usually obtained via state estimation[10] or time-domain solutions of the swing equation[11]. While recent efforts have focused on capturing time-synchronized rotor angles measurements to improve visibility[12], direct measurements remain scarce for existing applications. Most existing techniques rely on rotor angles estimated from synchrophasor measurements provided by PMUs[13-15]. However, many of these methods utilize linearized swing equations during disturbances[11], which can lead to erroneous estimations during the highly non-linear transient phase.

To address these challenges, this paper utilizes the "Phasor Area Criterion" (PAC) to quantify the transient stability status and identify out-of-step generators using positive sequence voltage phasors (V_{+ve_seq}) from PMUs. The PAC is employed here to assess transient stability in the context of IBR integrated power systems, specifically investigating the impact of grid following with/without inertial control. The PAC utilizes a monotonically increasing parameter to quantify stability, effectively eliminating false triggers caused by multiple threshold crossovers. Inspired by the well-known Equal Area Criterion (EAC), it provides an intuitive visual assessment based on the trajectories of (V_{+ve_seq}).

The performance of PAC is validated across multiple scenarios, including IBR integrated two-area power system, the 8th January 2021 ENTSO-E separation event. The results demonstrate the effectiveness of PAC for the assessment of transient stability for power systems integrated with IBRs.

2. PHASOR AREA CRITERION

The concept of Phasor Area Criterion has been previously reported in[16], and is utilized for IBR integrated systems. The Phasor Area Criterion is presented for a single machine infinite bus system as given in Figure 1. A symmetrical transmission line fault is applied at θ_o instance and cleared at θ_{cl}. The $\vec{V}_m$ phasor (green phasors) shows the pseudo measurements from PMU, whereas $\vec{V}_o$ (purple phasors) shows phasors during fault whose magnitude is projected onto pre-fault steady state voltage ($\vec{V}_{PS}$). During the fault interval ($t_o < t < t_{cl}$), the rotor accelerates, and it gains kinetic energy. The acceleration of the rotor is reflected in the increasing values of $\vec{V}_{+ve_seq}$ (Positive sequence voltage) angles. As the $\vec{V}_{+ve_seq}$ angles can mimic the

rotor angles, the area covered during the fault interval will be a function of area A, i.e., f(A). Similar to the area A_1 in EAC, the area $f(A_1)$ in PAC will be greater for the larger fault clearing angle θ_{cl}. In comparison, a larger value of fault resistance R_f (less severe fault) would lead to a decreased value of $f(A_1)$.

For power utilities, the practical expectation is therefore not a single detection technique, but a layered sensor that can: (i) recognize known vulnerabilities and malware patterns, (ii) detect unusual activity on non-deterministic devices, and (iii) validate deterministic IEC 61850 communications against engineering intent and protocol conformance[1,2].

θo	=	$\vec{V}_{+ve\ seq}$ angle pre-fault
θcl	=	$\vec{V}_{+ve\ seq}$ angle at fault clearing
θmax	=	$\vec{V}_{+ve\ seq}$ angle at transient stability limit $\theta max = \pi - \theta o$
θm	=	maximum $\vec{V}_{+ve\ seq}$ angle swing after an event
$f(A_1)$	=	$\theta m < \theta max$ for stability $\theta m > \theta max$ for instability a → b → c → d → a
$f(A_2)$	=	c → d → e → o → c
$\vec{V}m$	=	$\vec{V}_{+ve\ seq}$ measured phasors (green vector)
$\vec{V}o$	=	$\vec{V}_{+ve\ seq}$ voltage phasor projected with $\lvert\vec{V}_{P\ S}\rvert$ magnitude for fault duration (purple vector)
$\vec{V}cl$	=	$\vec{V}_{+ve\ seq}$ voltage phasor measured at fault clearing time
$\vec{V}PS$	=	$\vec{V}_{+ve\ seq}$ pre-fault steady state voltage phasor

After fault clearing at θ_{cl}, the synchrophasor angles keep on increasing due to the rotor's moment of inertia, and it is reflected in increasing values of $\vec{V}_{+ve_seq}$ angles. Figure 1 shows the area f(A2) covered during post-fault clearing. If the event is severe enough to cause instability, $\vec{V}_{+ve_seq}$ angles may cross the θmax limit, thus, indicating a loss of synchronism in the system. The intuition behind PAC is that the area enclosed by the $\vec{V}_{+ve_seq}$ within the phasor plots post fault must be bounded within some area (ABOUND P AC) for the system to maintain its transient stability, i.e., the trajectory of the area swept must be converging in nature. Based on the previous discussion, the mathematical formulation for PAC is given in(1a), (1b), and (1c)

$$A_{NET\ P\ AC} = f(A_1) + f(A_2) \tag{1a}$$

$$A_{NET\ P\ AC} \leq A_{BOUND\ P\ AC} \Longrightarrow \text{Stability} \tag{1b}$$

$$A_{NET\ P\ AC} \geq A_{BOUND\ P\ AC} \Longrightarrow \text{Instability} \tag{1c}$$

The areas $f(A_1)$ and $f(A_2)$ shown in Figure 1, are represented in (2a) and (2b), respectively.

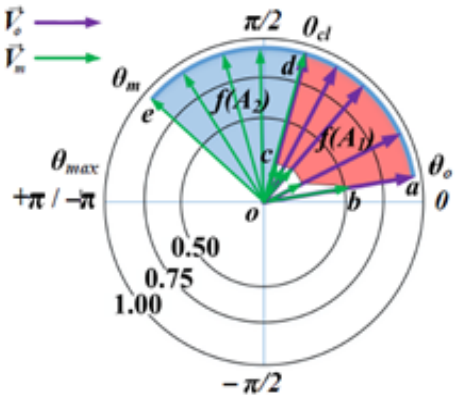


Figure 1. Illustration of phasor area criterion.

$$f(A_1) = \int_{\theta o}^{\theta cl} f\left(|\vec{V}_o|, \theta_o\right) dA - \int_{\theta o}^{\theta cl} f\left(|\vec{V}_m|, \theta_m\right) dA \tag{2a}$$

$$f(A_2) = \int_{\theta cl}^{\theta m} f\left(|\vec{V}_m|, \theta_m\right) dA \tag{2b}$$

where, dA = V dV dθ

The value of the A_{NET_PAC} given in (1a) is proportional to the severity of the event. For mathematical convenience, the areas and their bounds will be expressed with respect to a percentage base value. In the case of PAC, the base value is selected as the polar

plot's Total Area (TA). The values of p.u. voltage in power systems is close to 1. Therefore, the radius R of the polar plot is selected as 1. Hence, the polar plot's Total Area (TA) is calculated using (3).

$$TA = \pi \times R^2 = \pi \times 1^2 = \pi \quad (3)$$

The value ($\%A_{NET-PAC}$) is based on the percentage of the area enclosed by the ANET P AC in comparison to the total area of the phasor plot as given in (4).

$$\%A_{NET_{PAC}} = \frac{A_{NET_{PAC}}}{TA} \times 100 \quad (4)$$

The value of $A_{NET-PAC}$ given in (1a) can be used to assess if a generator can maintain transient stability after a disturbance. Suppose the $A_{NET-PAC}$ is within limits after a disturbance. In that case, a convergence criterion defined in (5) must be satisfied for T continuous seconds to confirm a generator's stability status as stable after a disturbance.

$$A_{NET_PAC}(t) = A_{NET_PAC}\,(t-1) \leq \epsilon_{conv} \quad (5)$$

t	=	t^{th} time instance
$ANET\ PAC\,(t)$	=	$f(A_1(t)) + f(A_2(t))$
$\epsilon conv$	=	convergence threshold
T	=	time in seconds

To implement PAC the two additional steps must be taken.

- The voltage phase angles must be referred to a common wide area reference.
- The area in (1a) must be implemented by utilizing a convex hull.

The readers are advised to read[16] for detailed implementation steps related to convex hull and wide area reference. The above two points are briefly explained as follows.

A. Wide Area Reference for PAC

The synchrophasor angles inherit clockwise or counter-clockwise rotation at off-nominal system. The speed of ro-tation for a j^{th} phasor is given by (6).

$$\Delta\omega_j = 2\pi(f_j - f_o) \quad (6)$$

where j = 1, 2, 3...L and L = a subset of N PMUs such that L < N.

To address the issues with incorrect calculations during off-nominal operation, a Wide Area Reference (WAR) phasor is created, which is based on the wide area average of the synchrophasor angles. Thus, the change in reference causes the measured phasors to maintain a relatively stationary angular position even at off-nominal frequencies. The WAR phasor is generated using synchrophasor angles from a few available PMUs at the generator buses that are located electrically far from the event while spreading evenly in the network.

Equation (7) shows the generation of WAR using the average of phasors V_j from L available PMUs as shown in Figure 2(a). $Re(V_j)$ and $Im(V_j)$, denotes the real and imaginary components of the $\vec{V}_{+ve_seq}$. Once the WAR reference is gen erated, changing the reference frame of the measured phasors to WAR is essential. Figure 2(b) shows the transformation of synchrophasor angles referred to WAR.

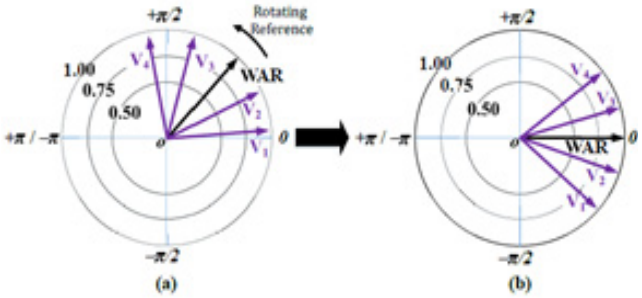


Figure 2. **(a)** Generation of WAR using measured phasors **(b)** Transformation of measured phasors with respect to WAR.

$$WAR_{Complex} = \frac{\sum_{k=1}^{L} Re(V_k H_k)}{\sum_{k=1}^{L} H} + j\frac{\sum_{k=1}^{L} Im(V_k H_k)}{\sum_{k=1}^{L} H_k} \quad (7)$$

B. Convex Hull for Calculating Area

The Quickhull algorithm is a method to compute the convex hull of a finite set of points in the plane. The convex hull is the smallest convex polygon that encloses all the points. The algorithm operates recursively by

finding extreme points and partitioning the set of points into subsets.

The solution of (2a) can be found using a convex hull that effectively captures the deviations for the $\vec{V}$+ve phasor measurements

Let V be a symbol to describe spaces, and let (x, y) be any two points in V. Various terms are defined as follows [17]:

Convex Combination let K∈ V , then the set of all convex combination of (x, y) is the set of points given by (8).

$$F(x,y) \in \mathbb{V} : F(x,y) = \lambda x + (1-\lambda)y, \lambda \in [0,1] \quad (8)$$

Convex Set Let K∈ V. Then the set K is said to be convex provided that given two points (x,y)∈ K, and the set in (8) is a subset of K

Convex Hull: There are enumerate number of sets that can form the convex set for the given non-convex set. Therefore, for a given set V⊂ C, the convex hull is defined as the intersection of all sets that contain C. Figure 3 shows an example of non-convex, convex, and convex hull set. For a comprehensive understanding of the convex hull technique, readers are encouraged to refer[17].

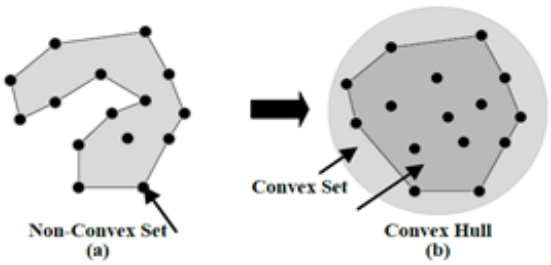


Figure 3. **(a)** Non-convex set, **(b)** Convex set and convex hull.

3. SYSTEM MODELING AND TEST CASE GENERATION

The simulations for stability assessment using Phasor Area Criterion are conducted in PSCAD/ EMTDC for on a modified two area power system as shown in Figure 4.

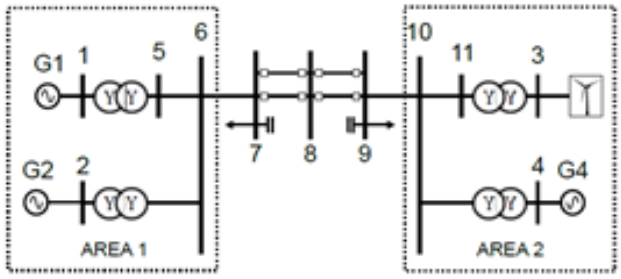


Figure 4. Modified two area power systems with IBR integration.

The synchronous generator at bus 3 from the traditional system is replaced with an IBR of an equivalent capacity of 700 MW. The PMUs are placed at the high voltage side of the terminals of the generators i.e., bus 5, 6, 10, and 11, respectively. Voltage phasors are recorded at 60 samples per second which can be streamed to a centralized PDC reporting to a control room for processing the measurements for transient stability assessment. The controls of the IBR are implemented using a grid following control with the ability to enable/disable inertial control. Test cases are generated with a load loss of 176 MW and 759 MW at bus 9, respectively. The frequency plots for stable cases given in Figure 5 indicate the better frequency response offered by the inertial control enabled IBR.

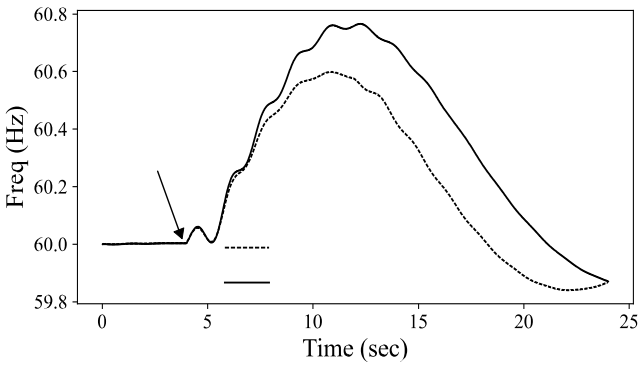


Figure 5. Frequency response due to 176 MW of load loss with/without inertial control for grid following.

4. RESULTS AND DISCUSSION

The simulated and practical cases are discussed for transient stability assessment with different converter

controls for contingencies leading to stability and instability:

A. Case A – Load loss of 176 MW at bus 9 without inertial control.

The system retains stability post load loss of 176 MW. Figure 6 shows the angles. It can be observed that post load loss, the phase angles converge indicating reduced stress on the tie line which is transferring power from area 1 to area 2.

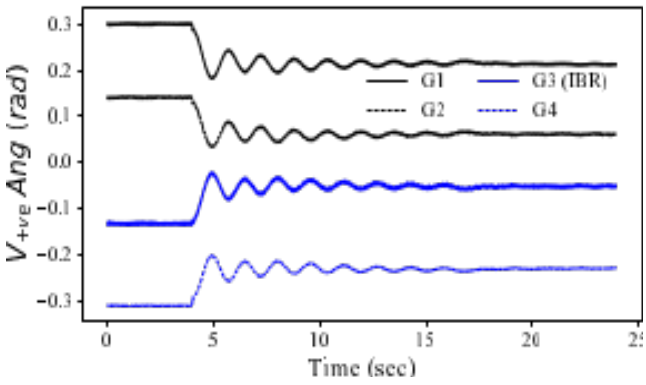


Figure 6. $\vec{V}_{+ve_seq}$ sequence phase angles for a load loss of 176 MW without inertial control.

To assess the transient stability, the index $\%A_{NET\ PAC}$ is estimated using voltage phasors, which is the area transversed by the trajectory of the $\vec{V}_{+ve_seq}$phasor. The timeseries plot for $\%A_{NET\ PAC}$ is given in Figure 7.

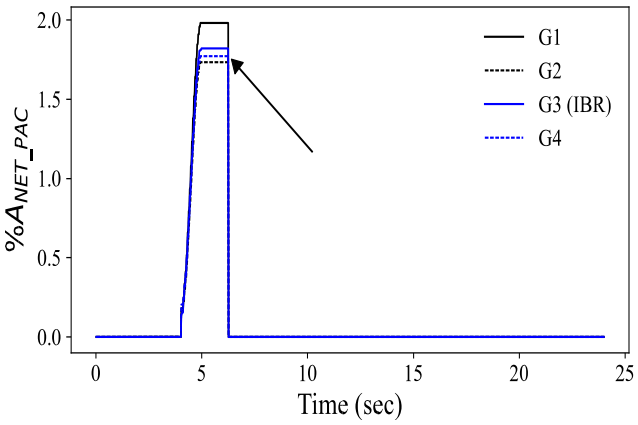


Figure 7. $\%A_{NET\ PAC}$ parameter for 176 MW load loss.

Table 1. $\%A_{NET}PAC$ VALUES AT t = 6.33 sec without inertial control

Unit	G1	G2	G3 (IBR)	G4
%A*NET PAC*	1.92%	1.68%	1.77%	1.71%

Unlike Figure 7, which shows $\%A_{NET\ PAC}$ values for all time instances, Figure 8 shows the $\%A_{NET\ PAC}$ values for each generating unit for a time instance of t = 6.33 sec, which is the instance of maximum area bounded by the voltage phasors.

Post satisfaction of (5), the values of $\%A_{NET\ PAC}$ are reset to zero, therefore indicating that the contingency is not severe enough to drive the system towards instability. Table 1 gives the quantitative values for each generating unit.

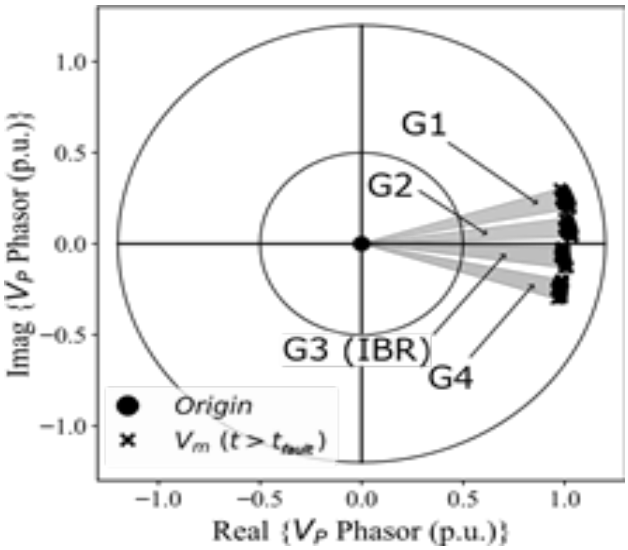


Figure 8. $\%A_{NET\ PAC}$ values for each generating unit for Case A.

B. Case B – Load loss of 176 MW at bus 9 with inertial control.

The IBR with inertial control offers a better frequency response. With the similar load loss, the stability assessment is conducted using Phasor Area Criterion. Figure 9 show the value of $\%A_{NET\ PAC}$ at the time instance t = 6.33 sec.

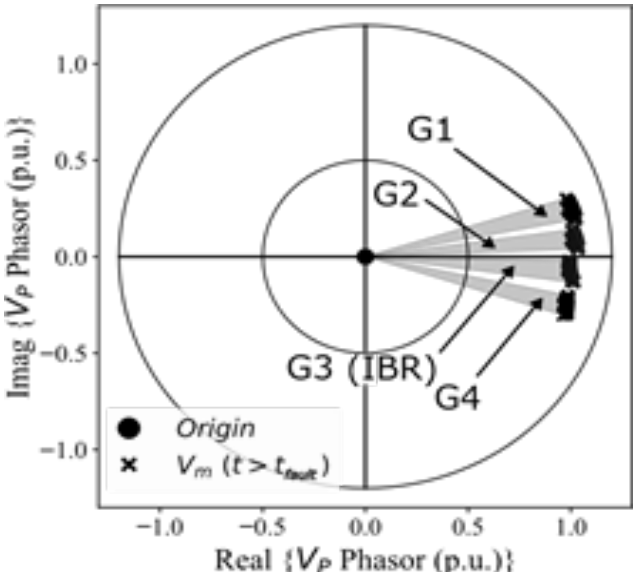


Figure 9. $\%A_{NET\,PAC}$ values for each generating unit for Case B.

Table 2 gives the quantitative values for each generating unit. It can be observed that the values of $\%A_{NET\,PAC}$ are ≈ 3% relatively lower with enabled inertial control. Therefore, indicating some improvement in stability margins. The inertial control injects active power relative to the Rate of Change of Frequency (ROCOF). Since, it is a stable contingency, the ROCOF may not be injecting large amount of active power in the system. Therefore, the index of $A_{NET\,PAC}$ is comparable for both control types. It is an interesting observation, and may require further studies to analyze the impact of inertial control on the transient stability assessment for IBR integrated systems.

Table 2. $\%A_{NET}PAC$ VALUES AT t = 6.33 SEC with inertial control

Unit	G1	G2	G3 (IBR)	G4
%A*NET PAC*	1.98%	1.73%	1.82%	1.77%

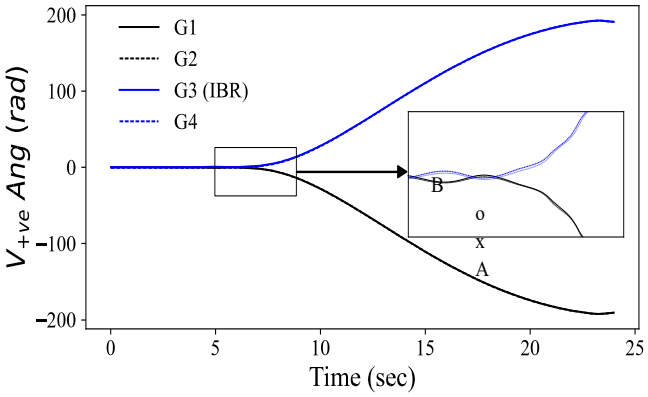


Figure 10. $\vec{V}_{+ve_seq}$ sequence phase angles for a load loss of 759 MW without inertial control.

A load loss of 759 MW is simulated at bus 9. Figure 10 shows the $\vec{V}_{+ve_seq}$ angles, the diverging nature of the angles indicates that post load loss the system becomes unstable.

C. Case C – Load loss of 759 MW at bus 9 without inertial control

Figure 11 shows the $\%A_{NET\,PAC}$ values for each generating unit for a time instance of t = 7.3166 sec, which is the instance of area bounded by the voltage phasors greater than 50% of the total area given in (4). The values of $\%A_{NET\,PAC}$ indicate that the contingency is severe enough to drive the system towards instability. Table 3 gives the quantitative values for each generating unit.

Table 3. $\%A_{NET}PAC$ values AT t = 7.3166 SEC with inertial control

Unit	G1	G2	G3 (IBR)	G4
%A*NET PAC*	40.80%	36.30%	52.07%	47.41%

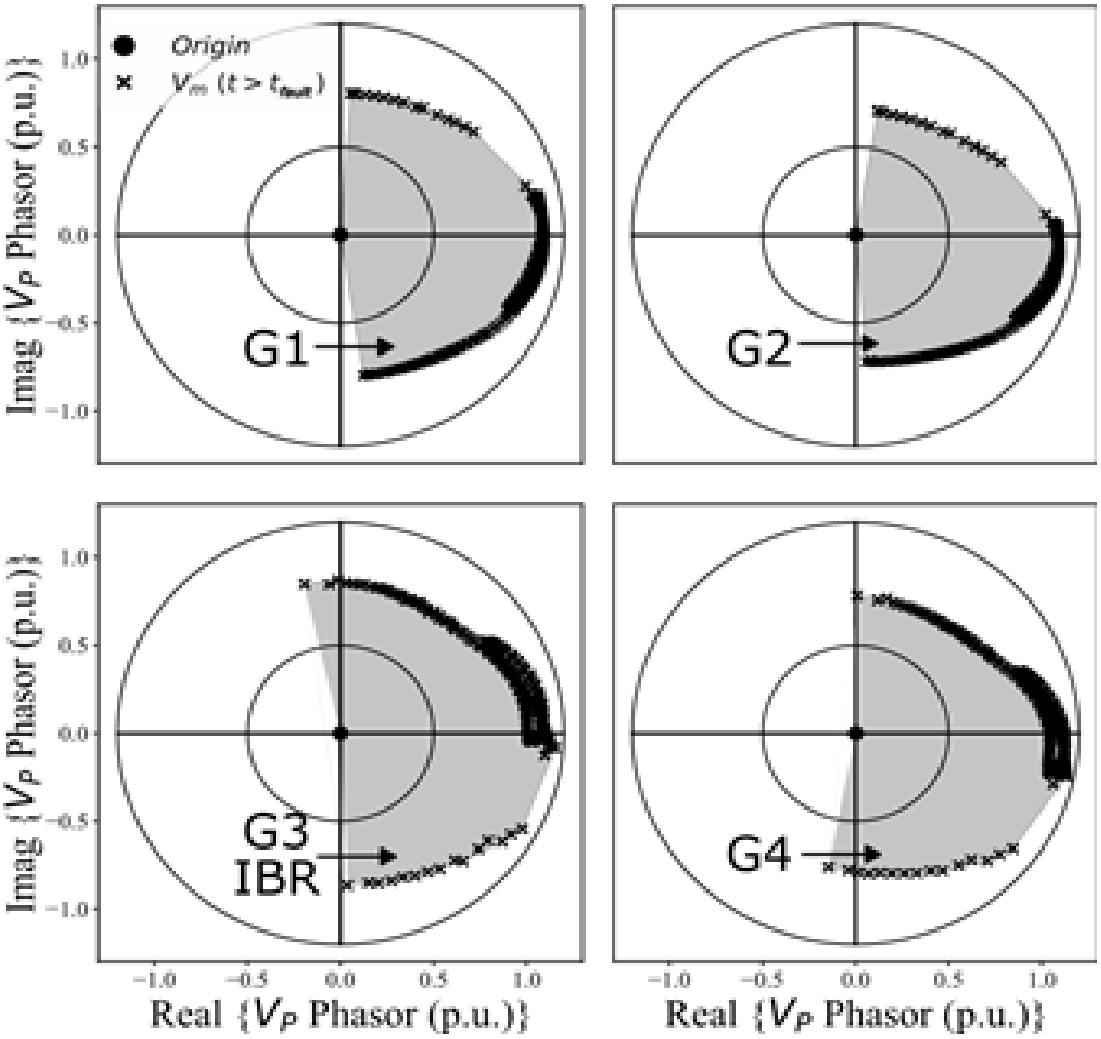


Figure 11. For the contingency of 759 MW, the IBR with inertial control also results in an unstable system. Therefore, the results for inertial control enabled IBR is omitted.

D. Case D – ENTSO-E Grid Separation (Near Miss Blackout)

On 8th January 2021, the ENTSO-E encountered a severe grid contingency that led to the separation of the European grid into two parts (North-West: Power deficit and South-East: power surplus) as shown in Figure 12 split of the regions[7].

The two major events that lead to the separation of the ENTSO-E grid are given as follows. Events 1 (instance A and instance B) were the opening of a bus bar coupler and overload protection of both 440/110 kV transformer at the Ernestinovo substation as shown in Figure 13. Figure 13(d) shows that for event 1 the $\%A_{NET\ PAC}$ parameter has the highest value for Ernestinovo substation, hence, it is correctly able to identify the source. Even though the voltage dip for event 1 is greater for Subotica Substation, the $\%A_{NET\ PAC}$ parameter for Ernestinovo substation is the highest. Thus, giving the system operators preemptive information that the localization of grid stresses and that could be useful to prompt grid operators in taking suitable preventive measures before the system encountered event 2, which was a tripping of Novi Sad-Subotica line which led to $N-1$ contingency violation[7].

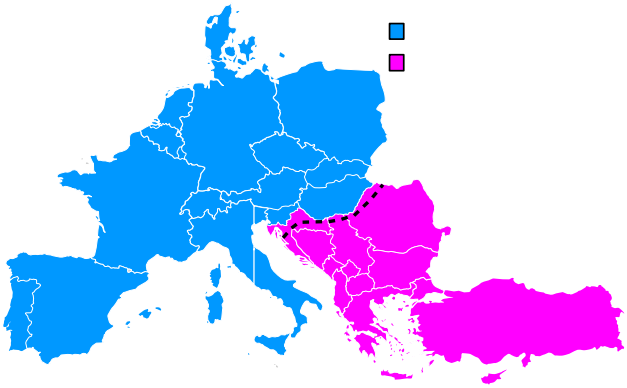


Figure 12. 8th January 2021 grid separation event for the ENTSO-E grid.

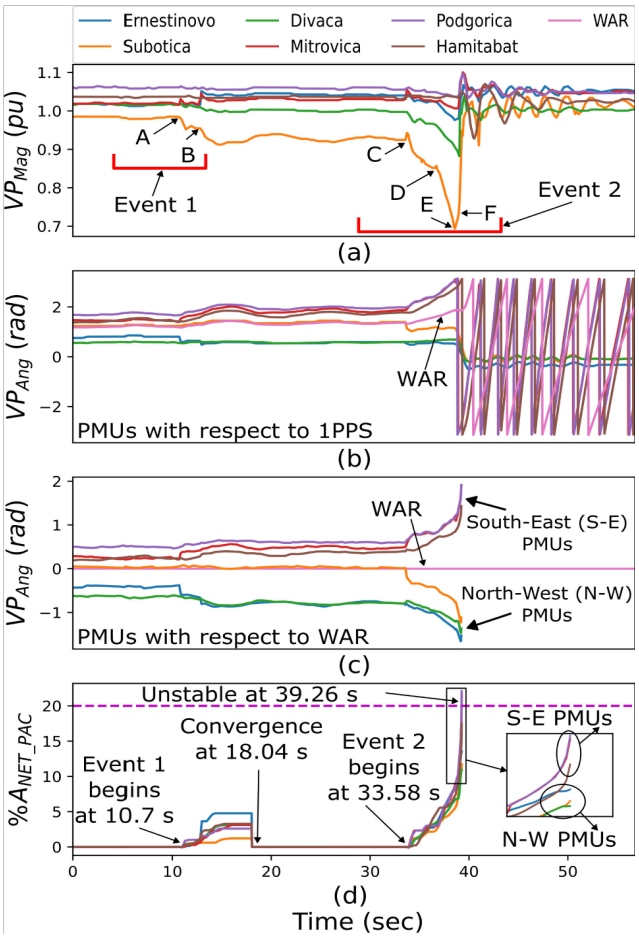


Figure 13. ENTSO-E 8th January system separation **(a)** Positive sequence voltage magnitude, **(b)** Positive sequence voltage phase angles with respect to 1PPS, **(c)** Positive sequence voltage phase angles with respect to WAR, and **(d)** $\%A_{NET}PAC$ for the event.

5. CONCLUSION

The paper presents a method for the assessment of transient stability for power systems integrated with IBRs (inertial and non-inertial control). The stability of the modified test systems is assessed using Phasor Area Criterion. The criterion provides a quantitative measure of stability margins for any grid event. Thus, it enables the assessment of contingencies regardless of whether the system remains stable or experiences an actual N −1 violation. The $\%A_{NET\ PAC} \approx 2\%$ parameter remains low and bounded for stable contingencies, whereas for unstable cases, the $\%A_{NET\ PAC}$ quickly becomes unbounded and rises above ≥ 50% for contingencies with N−1 violations. Therefore, indicating a useful parameter to grid operators for real-time assessment of transient stability margins. It is observed that the transient stability margins can potentially be improved with added inertial control. However, requiring further studies to identify the limits of inertial control for improving the stability margins. The results for practical grid data for the 8th January 2021 system separation event for the European grid indicates the real-time benefits to grid operators for prompt actions and situational awareness.

6. REFERENCES

1. Abdelilah Y, *et al.*, Renewables 2020: Analysis and Forecast to 2025. Technical report, International Energy Agency; 2020.
2. Central Electricity Regulatory Commission, India. Report on the Grid Disturbances on 30th July and 31st July 2012. Technical report; August 2012.
3. Final report on the August 14, 2003 blackout in the United States and Canada: causes and recommendations.
4. Union for the co-ordination of transmission of electricity. System Disturbance on 4 November 2006. Technical report; January 2007.
5. Liu Y, Singh AK, Zhao J, *et al.*, Dynamic State Estimation for Power System Control and Protection. IEEE Trans. Power Syst. 2021; 36(6):5909-5921. https://doi.org/10.1109/TPWRS.2021.3079395

6. Hatziargyriou H, Milanovic J, Rahmann C, *et al.* Definition and classification of power system stability - revisited and extended. IEEE Trans Power Syst. 2021; 36(4):3271-3281. https://doi.org/10.1109/TPWRS.2020.3041774

7. European network of transmission system operators for electricity. Continental Europe Synchronous Area Separation on 08 January 2021. Technical report; July 2021.

8. European network of transmission system operators for electricity. Continental Europe Synchronous Area Separation on 24 July 2021. Technical report; July 2021.

9. Pomarico A, Berizzi A, Guido R. Moraes, Issicaba D, Ildemar C. Decker. Countdown to collapse: Stability dynamics observed before the 2025 iberian power system blackout. In 2025 AEIT International Annual Conference (AEIT); 2025. p. 1-6 https://doi.org/10.23919/AEIT67669.2025.11218068

10. Zhao J, Netto M, and Mili L. A robust iterated extended kalman filter for power system dynamic state estimation. IEEE Trans Power Syst. 2017; 32(4):3205-3216. https://doi.org/10.1109/TPWRS.2016.2628344

11. Alinezhad B, Karegar HK. Out-of-step protection based on equal area criterion. IEEE Transactions on Power Systems. 2017; 32(2):968-977.

12. Rahman T, Sankaran S, Seeley N, Garg K. Capturing generator rotor angle and field quantities – SDG and experience and approach to using nontraditional generator measurements. In 2016 69th Annual Conference for Protective Relay Engineers (CPRE); 2016. p. 1-9. https://doi.org/10.1109/CPRE.2016.7914880

13. Wei S, Yang M, Qi J, Wang J, Ma S, Han X. Model-free MLE estimation for online rotor angle stability assessment with PMU data. IEEE Trans Power Syst. 2018; 33(3):2463-2476. https://doi.org/10.1109/TPWRS.2017.2761598

14. Siddiqui SA, Verma K, Niazi KR, Fozdar M. Real-time monitoring of post-fault scenario for determining generator coherency and transient stability through ANN. EEE Trans Ind Appl. 2018; 54(1):685-692. https://doi.org/10.1109/TIA.2017.2753176

15. Azman SK, Isbeih YJ, Moursi MSC, Elbassioni K. A unified online deep learning prediction model for small signal and transient stability. IEEE Trans Power Syst. 2020; 35(6):4585-4598. https://doi.org/10.1109/TPWRS.2020.2999102

16. Iqbal A, Jain T. Phasor area criterion - wide area assessment of transient stability. IEEE Trans Power Syst. 2024; 39(6):6876-6888. https://doi.org/10.1109/TPWRS.2024.3370843

17. Boyd S and Vandenberghe L. Convex Optimization. Cambridge